

Screening of False Induction Motor Fault Alarms Produced by Axial Air Ducts Based on the Space-Harmonic-Induced Current Components

Chanseung Yang, *Student Member, IEEE*, Tae-June Kang, *Student Member, IEEE*, Sang Bin Lee, *Senior Member, IEEE*, Ji-Yoon Yoo, Alberto Bellini, *Member, IEEE*, Luca Zarri, *Senior Member, IEEE*, and **Fiorenzo Filippetti**, *Member, IEEE*

Abstract—Motor current signature analysis (MCSA) based on the 50/60-Hz sidebands has become a common test in industry for monitoring the condition of the induction motor rotor cage. However, many cases of unnecessary motor inspection or outage due to false alarms produced by rotor axial duct interference have been reported. If the number of *axial ducts* and *poles* is identical, this can produce 50/60-Hz sideband frequency components in MCSA that overlap with that of rotor faults, resulting in false alarms. However, there currently is no practical test method available for distinguishing rotor faults and false indications other than testing the rotor offline or under the startup transient. In this paper, the feasibility of using the rotor fault frequency component produced by the space harmonic waves is evaluated as a solution for the first time. Since the fifth or seventh space harmonics have a spatial distribution of flux that does not penetrate in the rotor yoke to reach the axial ducts, they do not produce false alarms. The proposed method is verified on 6.6-kV motors misdiagnosed with broken bars via the 50/60-Hz sidebands of MCSA. It is shown that it provides reliable online indication of rotor faults independent of axial duct influence and can be used for screening out false alarms.

Index Terms—Condition monitoring, fault diagnosis, frequency-domain analysis, induction motor, predictive maintenance.

NOMENCLATURE

N_p, N_d Number of poles and rotor axial air ducts.
 N_s, N_r Number of stator and rotor slots.
 f_s Supply electrical frequency in hertz.

Manuscript received January 27, 2014; revised April 11, 2014 and May 13, 2014; accepted May 20, 2014. Date of publication June 13, 2014; date of current version February 6, 2015. This work was supported in part by the Basic Science Research Program through the National Research Foundation of Korea (NRF) funded by the Ministry of Education, Science and Technology (NRF-2013R1A1A2010370) and in part by the Human Resources Development Program (20134030200340) of the Korea Institute of Energy Technology Evaluation and Planning (KETEP) grant funded by the Ministry of Trade, Industry and Energy of Korea.

C. Yang, T.-J. Kang, S. B. Lee, and J.-Y. Yoo are with Korea University, Seoul 136-701, Korea (e-mail: y1c2s@korea.ac.kr; magnuskt@korea.ac.kr; sangbinlee@korea.ac.kr; jyoo@korea.ac.kr).

A. Bellini, L. Zarri, and F. Filippetti are with the University of Bologna, 40126 Bologna, Italy (e-mail: a.bellini@unibo.it; luca.zarri2@unibo.it; fiorenzo.filippetti@unibo.it).

Color versions of one or more of the figures in this paper are available online at <http://ieeexplore.ieee.org>.

Digital Object Identifier 10.1109/TIE.2014.2331027

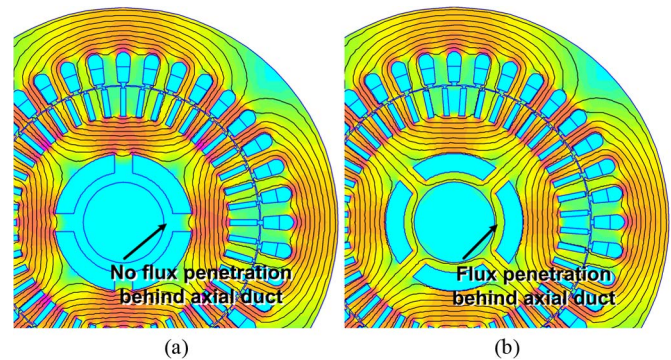


Fig. 1. FE analysis of flux distribution in the four-pole motor with four axial air ducts ($N_d = N_p = 4$) when magnetic poles and duct arms are electrically (a) 90° apart and (b) aligned (0°) under steady-state operation. The asymmetry in magnetic flux path produces false rotor fault alarm.

h h th space harmonic order.
 s Rotor slip.
 $f_{\text{duct}}, f_{\text{brb}, h}$ MCSA frequency sidebands produced by axial duct and broken bar due to h th space harmonic in hertz.
 k, m Positive integers.
 i_s, i_m, i_r Stator, magnetizing, and rotor currents.
 ϕ_e Electrical angle of broken bar location measured with respect to the axial duct in the direction of rotor rotation.
 $f_h, f_{h,r}$ Frequency (speed) of h th order space harmonic wave with respect to stator and rotor in hertz.
 $k_{p,h}$ Stator pitch factor for h th space harmonic component.

I. INTRODUCTION

MOTOR current signature analysis (MCSA) is one of the most popular tools for monitoring the condition of the rotor cage of medium-voltage/high-voltage (MV/HV) induction motors. The online and remote monitoring capability of MCSA makes it an attractive and convenient technology in an industrial environment [1]–[6]. However, false rotor fault alarms for healthy motors can be caused by rotor axial ducts, rotor ovality, low-frequency load oscillations, or porosity (aluminum die cast rotors) when the 50/60-Hz sidebands are used, as reported in [4]–[11]. A false alarm can result in an unnecessary and costly inspection or outage of the motor and driven process. The cost

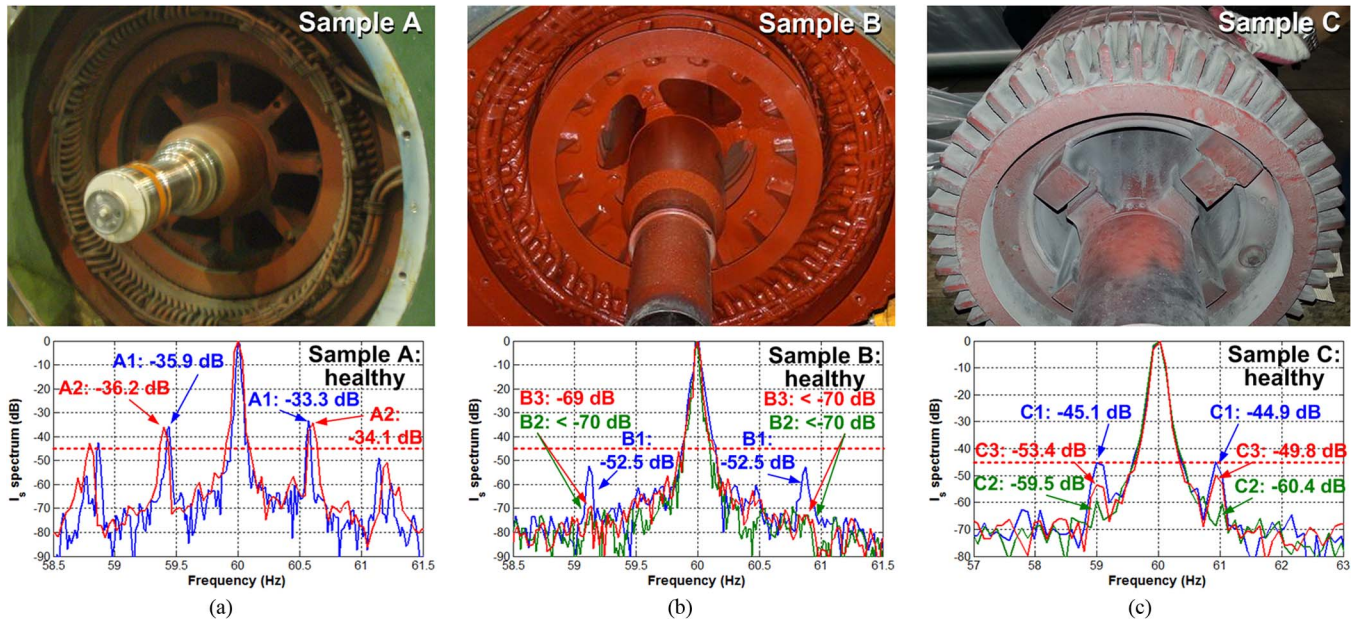


Fig. 2. Rotor (upper) and stator current I_s spectrum (lower) of 6.6-kV motors with identical number of rotor air ducts N_d and poles N_p with false rotor fault alarms produced with MCSA. (a) Sample A (A1, A2): 2400-kW eight-pole-induced draft fan motor ($N_d = N_p = 8$). (b) Sample B (B1, B2, B3): 280-kW four-pole condensate pump motor ($N_d = N_p = 4$). (c) Sample C (C1, C2, C3): 350-kW four-pole condensate pump motor ($N_d = N_p = 4$).

of inspection for MV/HV motors with a false alarm is typically tens of thousands of dollars, excluding the cost of repair and loss of production (if standby or spare motors are available) [9]–[11].

One of the most common root causes of false rotor fault alarms is the interference caused by rotor axial air ducts. Rotor air ducts, shown in Fig. 1, are employed in motors rated above 100 kW for effective cooling of the rotor and reduction in inertia and material costs [9], [10]. Axial ducts can cause the magnetic reluctance of the flux path to be asymmetric since the flux can penetrate the inside of the axial ducts depending on the relative position between the flux and rotor, as illustrated in Fig. 1. The difference in the flux path can be seen in the results of the 2-D finite-element (FE) analysis in Fig. 1(a) and (b) for a four-pole motor with four axial ducts [high-reluctance path in Fig. 1(a) and low-reluctance path in Fig. 1(b)]. The variation in the magnetic reluctance results in modulation of the magnetizing current i_m , whereas the variation in rotor resistance due to broken bars produces modulation in the rotor current i_r . Modulation of i_m can produce components at f_{duct} in the current spectrum that are identical to the rotor fault frequency $f_{\text{brb},1}$ if the number of air ducts N_d and poles N_p are the equal as

$$f_{\text{duct}} = f_{\text{brb},1} = (1 \pm 2ks)f_s \quad (1)$$

where f_s is the supply frequency, s is the rotor slip, and k is a positive integer. This can be misinterpreted as broken rotor bars when the 50/60-Hz sideband-based MCSA (hereinafter referred to as MCSA) is applied, as reported in [5]–[11].

Three recent cases of false MCSA rotor fault alarms produced by the axial duct influence are shown in Fig. 2 for 6.6-kV induction motors [9]–[11]. The results of MCSA performed on the three motor samples (samples A, B, and C)

indicated broken bars in some of the rotor samples. However, inspection of the rotors showed that the bars are in healthy condition for all motor samples. This resulted in unnecessary expenditures for the inspection, where the cost of inspection alone exceeded 100 000 dollars for the 2.4-MW motor of Fig. 1(a). False MCSA alarms due to axial ducts are a common on-going problem in the field, considering that a large portion of MV/HV motors are of $N_d = N_p$ design, according to the investigation in [9]. In most cases, it is unknown whether a motor is of $N_d = N_p$ design unless the motor is disassembled. If a motor is of $N_d = N_p$ design, it does not necessarily produce the $f_{\text{brb},1}$ component since this depends on the rotor design and construction, material characteristics, and operating conditions [9].

A number of researchers have worked on separating the influence of the rotor fault and air duct in [5]–[10] for screening out false alarms to prevent unnecessary and costly motor inspection. In [5]–[7], it is suggested that the $f_{\text{brb},1}$ component be compared under two different load conditions. Since it is the modulation of the magnetizing current that produces the false indication, the $f_{\text{brb},1}$ components decrease with increase in load if produced by axial ducts. Although this could screen out false alarms for healthy motors, it cannot provide reliable assessment for faulty motors, as will be shown in Section II. In [8], a method for separating the two effects online based on a mathematical model was proposed. However, the requirement of data under multiple load conditions is not feasible for many industrial applications and is a limitation of the methods presented in [5]–[8]. In [9]–[11], it is shown that broken bars can be detected reliably independent of axial ducts if tested under high-slip (offline standstill [9] and startup transient [10]) conditions since there is no flux penetration in the rotor (cage eddy current rejection), as shown in Fig. 3(a). The limitation of the offline tests is the requirement of motor disassembly

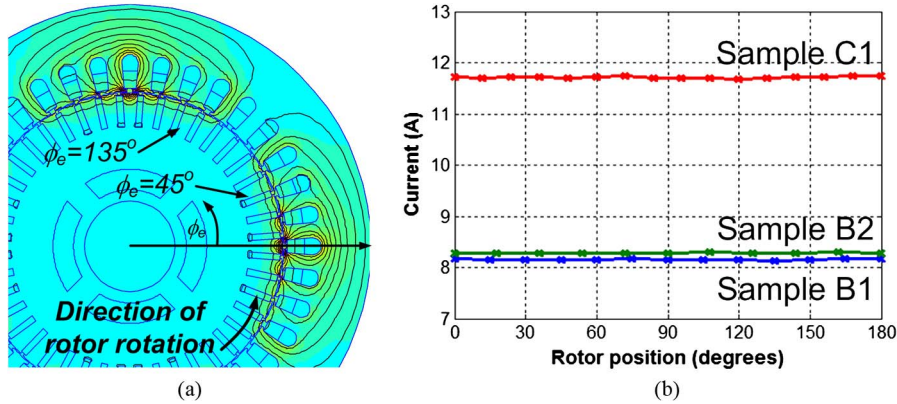


Fig. 3. (a) FE analysis of flux distribution under 60-Hz excitation at motor standstill. (b) Single-phase rotation test results (current versus rotor position) on samples B1, B2, and C1 under 380-V pulsating field excitation at motor standstill.

or manual shaft rotation for testing, which makes frequent, automated, and remote motor testing difficult [12]. It is also difficult to perform a startup test for applications that are run continuously.

It is clearly shown in the analysis presented in [9] and the aforementioned arguments that a false alarm due to axial ducts is common and the consequence can be serious. It is also shown in [9]–[11] that there currently is no practical method available for screening out false alarms when the motor is operating. Based on the fact that the space harmonic flux cannot penetrate into the air ducts to produce asymmetry, the objective of this paper is to investigate the feasibility of using the space-harmonic-induced rotor fault components. An experimental study on custom-built 380-V and 6.6-kV motors with false alarms shows that the proposed method provides reliable detection of rotor faults independent of the axial duct influence.

II. INFLUENCE OF ROTOR AXIAL AIR DUCTS ON MCSA

A. False Rotor Fault Alarms—Case Studies

The MCSA results of the stator current I_s spectrum for the healthy 6.6-kV motors ($N_d = N_p$) with false broken bar alarms are shown in Fig. 2. The three 6.6-kV motors in Fig. 2(a)–(c), denoted as samples A, B, and C, are fan or pump motors operating in power generation plants. For the critical HV motors in power plants, multiple motors are operated in parallel to share the load, and standby motors of identical design are often installed to minimize the impact of motor failure. MCSA measurements for samples A, B, and C were obtained from all of the identical motor units available. The ratings, application, and figure where test results are shown are summarized in Table I. For the 2400-kW-induced draft fan motor, both samples A1 and A2 showed strong $f_{brb,1}$ sidebands between -37 and -33 dB, respectively, in the current spectrum [Fig. 2(a)]. This exceeds the -45 -dB fault threshold level commonly used in the field. Vibration analysis also indicated rotor faults; however, motor inspection did not reveal any signs of rotor bar or end ring damage.

For the 280- and 350-kW condensate pump motor samples B and C, the MCSA measurements of the $f_{brb,1}$ components for three identical units were not consistent, as can be seen in Fig. 2(b) and (c). The $f_{brb,1}$ components were -52.5 dB for

TABLE I
RATINGS, APPLICATION, AND TEST RESULTS FOR FIELD AND LABORATORY MOTOR SAMPLES

| Sample | P (kW) | V (V) | N_d / N_p | Application | Rotor Photo (Fig.) | MCSA $f_{brb,1}$ (Fig.) | MCSA $f_{brb,5}$ (Fig.) |
|-----------|--------|-------|-------------|-------------------|--------------------|-------------------------|-------------------------|
| A (A1~A2) | 2400 | 6600 | 8 | Induced draft fan | 2(a) | 2(a) | - |
| B (B1~B3) | 280 | 6600 | 4 | Condensate pump | 2(b) | 2(b), 15 | 15(a) |
| C (C1~C3) | 350 | 6600 | 4 | Condensate pump | 2(c) | 2(c), 15 | 15(b) |
| D | 5.5 | 380 | 4 | Laboratory | 7(a) | 8 | 9, 10 |
| E | 5.5 | 380 | 4 | Laboratory | 7(b)-(c) | 11 | 12-13 |
| F(F1,F2) | 5.5 | 380 | 0/4 | Laboratory | - | 14 | 14 |

sample B1 and below -69 dB for samples B2 and B3. For samples C1, C2, and C3, the $f_{brb,1}$ components were spread out between -45 and -60 dB, as shown in Fig. 2(c). Rotor faults were strongly suspected for samples B1 and C1 considering that the $f_{brb,1}$ components were significantly higher than those of the motors of identical design. Since the sample B1–B3 and C1–C3 motors were manufactured and commissioned at the same time and operated under similar load, it was natural to conclude that it is very unlikely for the motors to have larger $f_{brb,1}$ components unless a rotor fault is present. However, the results of offline inspection and testing showed that both rotors for samples B1 and C1 were in good condition.

The single-phase rotation test was performed on samples B1, B2, and C1 with 380 V applied between two terminals for pulsating field excitation [12]. The results of the current measurements as a function of the rotor position shown in Fig. 3(b) imply that there is no asymmetry in the rotor cage. If a broken bar is present, the current fluctuates N_p times, as the rotor is rotated one revolution due to the variation in the rotor impedance. The reason why the single-phase test is not influenced by the axial ducts is the limited flux penetration into the rotor yoke under standstill conditions, as shown in Fig. 3(a). The inconsistency in the $f_{brb,1}$ components for samples B and C is suspected to be caused by part-to-part variation introduced due to component or manufacturing tolerances such as the variance in the Si-Fe lamination magnetic characteristics [9]. It was concluded based on the inspection and test results that the false-positive indication for samples A, B, and C was due to the axial air ducts for the $N_d = N_p$ motors.

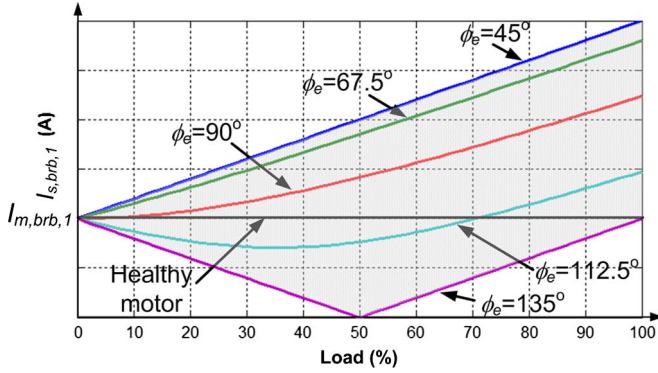


Fig. 4. Example of the values of $I_{s,brb,1}$ as a function of slip (load) for different ϕ_e values calculated from (3) for a faulty rotor (assuming that $I_{m,brb,1} = 2I_{r,brb,1}$).

B. Screening of False Alarms Due to Axial Air Duct Influence

It is difficult to screen out false MCSA rotor fault alarms because the axial ducts and broken bars produce the same frequency component in the stator current when performing MCSA. The two components interact since the $f_{brb,1}$ components measured in the stator current $i_{s,brb,1}$ are the sum of the two current components shown in

$$i_{s,brb,1} = i_{m,brb,1} + i_{r,brb,1}. \quad (2)$$

The $f_{brb,1}$ components produced by the axial ducts $i_{m,brb,1}$ and by the broken bars $i_{r,brb,1}$ have a different phase angle depending on the location of the fault with respect to the axial duct. The electrical angle measured with respect to the center of the axial duct in the direction of rotor rotation is denoted as ϕ_e , shown in Fig. 3(a). It was shown in [9] that the magnitude of $i_{s,brb,1}$ is a function of the magnitudes of $i_{m,brb,1}$, $i_{r,brb,1}$, rotor slip, and angle ϕ_e , as shown in

$$I_{s,brb,1} = \sqrt{I_{m,brb,1}^2 + 2I_{m,brb,1}I_{r,brb,1}s \sin(2\phi_e) + I_{r,brb,1}^2 s^2}. \quad (3)$$

A simulation was performed to illustrate how the values of $I_{s,brb,1}$ vary with fault location ϕ_e , as shown in Fig. 4. The values of $I_{s,brb,1}$ as a function of slip were calculated from (3) for a number of different values of ϕ_e . In Fig. 4, it was assumed that $I_{m,brb,1} = 2I_{r,brb,1}$ based on the ratio observed for samples D and E (shown in Section IV) when 1 of 44 bars is broken. It can be clearly seen in Fig. 4 and (3) that $f_{brb,1}$ components in the stator current are influenced significantly by the location of the rotor fault ϕ_e , in addition to the slip (load) and magnitudes of $i_{m,brb,1}$ and $i_{r,brb,1}$. The $I_{s,brb,1}$ component shows the maximum increase if the bar is broken at the $\phi_e = 45^\circ$ location, whereas it shows the maximum decrease when $\phi_e = 135^\circ$, as shown in Fig. 4. This is observed because the $i_{m,brb,1}$ and $i_{r,brb,1}$ components are in phase (add) when $\phi_e = 45^\circ$ and out of phase (cancel) when $\phi_e = 135^\circ$ [9]. If the fault is located at $\phi_e = 135^\circ$, $I_{s,brb,1}$ initially decreases but starts to increase if the magnitude of the $i_{r,brb,1}$ component exceeds that of $i_{m,brb,1}$. As a result, the $f_{brb,1}$ component measured in the current can be anywhere in the highlighted region of Fig. 4 depending on the slip (load) and ϕ_e for the

given $I_{m,brb,1}$ and $I_{r,brb,1}$. Therefore, the $f_{brb,1}$ component can increase, decrease, or remain unchanged if a broken bar is present in a $N_p = N_d$ motor with axial duct influence.

If a rotor fault alarm is given by MCSA, one must check if it is caused by a broken bar or axial ducts (false alarm). The easiest solution is to check N_d , if possible, to rule out the axial-duct-induced false alarm. Otherwise, the best option is to run an offline or startup test, but there are many limitations to performing these tests. The remaining options are to observe the trend of how the MCSA measurements change with load, time, or other motors of identical design. However, Fig. 4 and (3) clearly show that comparing the $i_{s,brb,1}$ magnitudes at two different loads suggested in [5]–[7] is invalid since $I_{s,brb,1}$ can decrease with an increase in load if the bar is broken in the vicinity of $\phi_e = 135^\circ$. Trending the values of $I_{s,brb,1}$ over time to observe an increase for broken bar indications is also invalid since $I_{s,brb,1}$ can decrease with a broken near $\phi_e = 135^\circ$. It can be seen from the MCSA results of samples B1–B3 and C1–C3 of Fig. 2(b) and (c) that comparison between motors of identical design cannot be used for screening out false alarms. The false rotor fault indication in samples B1 and C1 is not present for samples B2, B3, and C2 due to the variance in the characteristics of individual motors [9]. The case studies and analysis presented in this section clearly show that the $f_{brb,1}$ component does not provide sufficient information necessary for screening out false alarms due to axial ducts.

III. RELIABLE DETECTION OF ROTOR FAULTS BASED ON THE FIFTH-ORDER SPACE-HARMONIC-BASED MCSA COMPONENTS

It is clear from the arguments in Section II that MCSA cannot provide reliable detection of broken bars for $N_p = N_d$ motors. For such motors, rotor faults can only be detected reliably with offline standstill or startup transient tests, where the motor is excited under high-slip conditions [9], [10]. With high slip excitation, flux penetration in the rotor is limited due to cage eddy current rejection as shown in Fig. 3(a); therefore, the flux cannot reach the axial ducts. However, these tests cannot be performed online when the motor is running. Considering that the slip between the rotor and space harmonic flux is high, monitoring of the space-harmonic-induced rotor fault components is considered in this paper under the expectation that it is immune to false alarms due to axial ducts.

A. Rotor Fault Components Induced by Space Harmonics

It is shown in a number of resources that stator winding space harmonic waves produce rotor fault components $f_{brb,h}$ shown in (4) in the stator current spectrum when performing MCSA. The $f_{brb,h}$ sidebands can be observed for $k_2 = 5, 7, 11, 13, \dots$ if broken bars are present [4]

$$f_{brb,h} = (k_2(1-s) \pm s)f_s. \quad (4)$$

The nonideal (i.e., nonsinusoidal) distribution of the stator winding produces the fundamental component and a series

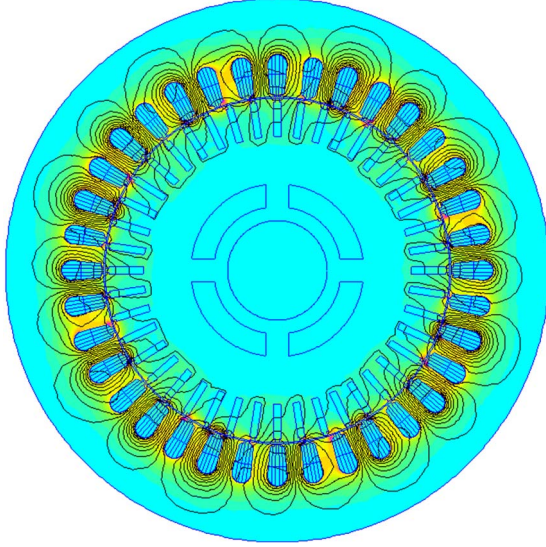


Fig. 5. Two-dimensional FE analysis of the fifth-order space harmonic flux distribution for the four-pole motor under rated slip operation.

of odd space harmonic h magnetomotive forces (MMF) in the machine, even for an ideal balanced three-phase sinusoidal input. The MMF contains space harmonics of order $h = 6m \pm 1$ ($m = 1, 2, \dots$), where MMFs rotate in the same (positive) direction as the fundamental wave for $h = 6m + 1$ ($h = 7, 13, \dots$) and in the opposite (negative) direction for $h = 6m - 1$ ($h = 5, 11, \dots$) as

$$h = \begin{cases} 6m+1 (\text{positive direction, } h=7, 13, \dots) \\ 6m-1 (\text{negative direction, } h=5, 11, \dots) \end{cases} \quad (m=1, 2, \dots). \quad (5)$$

The h th space harmonic MMF wave is equivalent to a machine with $h \cdot N_p$ poles considering the spatial distribution of flux. This can be seen in the FE analysis of the fifth-order harmonic flux distribution in a four-pole motor generated by splitting up the stator winding into that of a 20-pole stator in Fig. 5. The h th space harmonic wave rotates at a speed (frequency) f_h of $1/h$ of the fundamental wave as, shown in (6) [13], where the sign of $h - 6m$ represents the direction of rotation

$$f_h = (h - 6m)f_s/h. \quad (6)$$

The speed (frequency) of the space harmonic waves with respect to the rotor $f_{h,r}$ can be expressed as the difference between the speed of the h th space harmonic wave and rotor as

$$f_{h,r} = f_h - (1 - s)f_s. \quad (7)$$

It can be seen from (7) that the speed of the fundamental, fifth-order, and seventh-order space harmonic waves with respect to the rotor are sf_s , $-6/5f_s + sf_s$, and $-6/7f_s + sf_s$, respectively. This shows that the difference in the speed of the fifth and seventh space harmonic waves and the rotor is large compared to that of the fundamental wave. This results in high slip excitation of the rotor with $h \geq 5$ and makes penetration of the space harmonic flux into the rotor yoke difficult due to eddy current rejection of the rotor cage. It can be observed in the FE analysis of Fig. 5 that the fifth-order harmonic flux

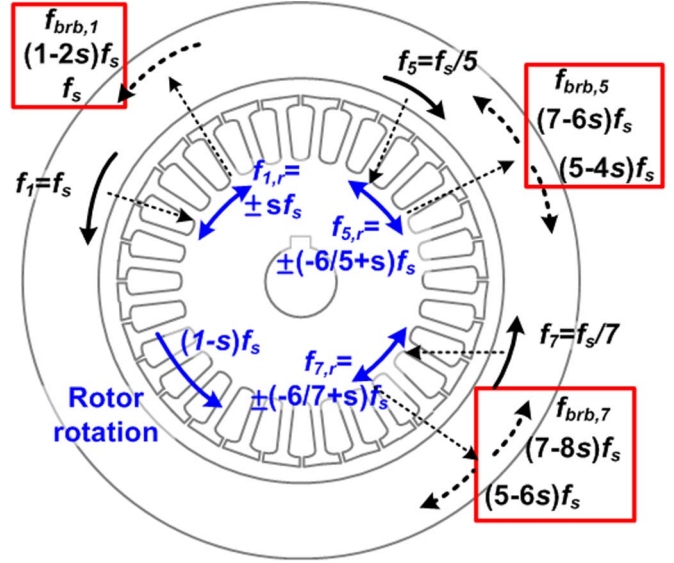


Fig. 6. Principle behind induction of $f_{br,b,h}$ components in the stator current for the fundamental, fifth, and seventh space harmonics.

TABLE II
SUMMARY OF f_h , $f_{h,r}$, AND $f_{br,b,h}$ FOR FUNDAMENTAL, 5TH, 7TH, 11TH, AND 13TH SPACE HARMONICS (+ REPRESENTS DIRECTION OF ROTOR ROTATION)

| h | f_h $(h-6m)f_s/h$ | $f_{h,r}$ $f_h - (1-s)f_s$ | $f_{br,b,h}$ $(1-s)f_s \pm f_{h,r}h$ |
|-----|------------------------|-------------------------------|---|
| 1 | f_s | sf_s | $(1-2s)f_s, f_s$ |
| 5 | $-f_s/5$ | $(-6/5+s)f_s$ | $-(5-4s)f_s, (7-6s)f_s$ |
| 7 | $f_s/7$ | $(-6/7+s)f_s$ | $-(5-6s)f_s, (7-8s)f_s$ |
| 11 | $-f_s/11$ | $(-12/11+s)f_s$ | $-(11-10s)f_s, (13-12s)f_s$ |
| 13 | $f_s/13$ | $(-12/13+s)f_s$ | $-(11-12s)f_s, (13-14s)f_s$ |

simulated to rotate at $-6/5f_s + sf_s$ does not reach the axial ducts and therefore does not produce false alarms as in the case of the fundamental wave shown in Fig. 1. This is similar to the reliable test methods such as the single-phase rotation test or startup transient test where the fundamental flux does not penetrate into the rotor yoke, as shown in Fig. 3(a). The space harmonic sideband-based MCSA has a significant advantage over existing methods in that it can provide reliable monitoring of the fault when the motor is operating.

If a fault is present in the rotor cage, the rotating fundamental and space harmonic fields create anomalies in the magnetic field that produce a pulsating field with respect to the rotor at frequencies of $f_{h,r}$ [4]. The pulsating field can be decomposed into two rotating fields in opposite direction ($\pm f_{h,r}$) according to the double revolving field theory. The h th space harmonic fields created by the fault induce $f_{br,b,h}$ frequency components in the stator winding in a manner similar to the fundamental wave as

$$\begin{aligned} f_{br,b,h} &= (1 - s)f_s \pm f_{h,r} \cdot h \\ &= \begin{cases} (1 - 6m) \cdot f_s + (h - 1) \cdot sf_s \\ (1 + 6m) \cdot f_s - (h + 1) \cdot sf_s \end{cases} \quad (8) \end{aligned}$$

where the equation is derived from (5)–(7). The principle behind the induction of the $f_{br,b,h}$ components in the stator current

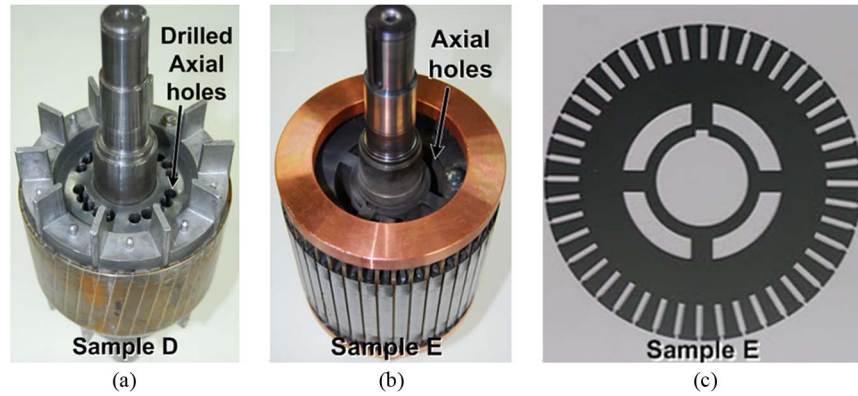


Fig. 7. (a) Al die-cast rotor with four drilled axial holes (sample D). (b) Fabricated Cu rotor with four laser cut axial holes (sample E). (c) Rotor lamination for sample E.

derived in (5)–(8) is illustrated in Fig. 6 for the fundamental, fifth, and seventh space harmonics. The frequencies of the h th space harmonic wave with respect to the stator and rotor (f_h and $f_{h,r}$) and the sideband components induced in the stator winding as a result of broken bars ($f_{brb,h}$) are summarized in Table II for the fundamental, 5th, 7th, 11th, and 13th space harmonics. The direction of rotor rotation is considered “positive” in the $f_{brb,h}$ components in Table II. It can be seen in Fig. 6 and Table II that the induction of the $f_{brb,h}$ components due to the space harmonics is the same, in principle, as that of the fundamental component. The $f_{brb,h}$ sidebands derived in (8) are identical to the components shown in (4) if MCSA is performed using one phase of the current, where the direction of rotation cannot be discerned. The flux distribution shown in Fig. 5 clearly shows that the $f_{brb,h}$ components can provide reliable detection of rotor faults, and the derivation of the $f_{brb,h}$ components is shown in Fig. 6 and Table II to support the analysis.

B. Expected Advantages and Limitations of the Proposed Method

The main advantage expected from monitoring the space-harmonic-related rotor fault components with MCSA is its immunity to the false alarms produced by axial ducts. The space-harmonic-induced $f_{brb,h}$ component can be monitored online during motor operation to screen out false alarms produced by the $f_{brb,1}$ sidebands commonly used. This provides a significant advantage over test methods that require the motor to be stopped for standstill testing or to be started to observe the transient. Monitoring of the space- or time-harmonic-induced sidebands has been studied in [14]–[19] for different purposes. In [14] and [15], the potential of using the $f_{brb,h}$ components for reliable detection of nonadjacent broken bars is evaluated. It is shown that nonadjacent broken bars separated 90 electrical degrees apart unobservable with the $f_{brb,1}$ component could be observed with $f_{brb,h}$ since the pattern of broken bars that are symmetrical to the fundamental flux is asymmetric to the space harmonic flux pattern. It is also shown that space- [16]–[18] or time-harmonic-based [19] detection of rotor faults is insensitive to load variations, inertia, or supply distortion or unbalance and is not influenced by load oscillations. The feasibility of using

this component for reliable fault detection independent of the influence of axial ducts is studied in this paper for the first time. The advantages of using the $f_{brb,h}$ component studied in [14]–[18] listed previously apply to the proposed method.

A potential shortcoming of monitoring the $f_{brb,h}$ component is the difficulty of determining the fault threshold. The fault threshold for the $f_{brb,1}$ component has been studied extensively in academia and determined based on experience accumulated in the field with MCSA technology over the years [4], [6], [20]–[22]. The $f_{brb,h}$ components will increase with fault severity; however, the degree of increase is expected to depend heavily on the magnitude of the specific space harmonic component in the stator winding. This depends on the winding design factors such as the pitch factor and distribution factor, which are unknown to the field maintenance engineer. Therefore, a reliable way of monitoring the rotor condition is to trend the increase in multiple $f_{brb,h}$ components over time and to observe it in conjunction with the $f_{brb,1}$ component.

IV. EXPERIMENTAL RESULTS

A. Experimental Setup

An experimental study was performed to verify the validity of space-harmonic-based MCSA for reliable monitoring of rotor faults independent of the axial duct influence. The proposed method was verified for the 6.6-kV field samples B and C and on custom-built laboratory samples D, E, and F. Two 380-V 5.5-kW motors with $N_d = N_p$ rotor samples (D and E) were custom built to verify the effectiveness of the method under controlled fault conditions in the laboratory. The axial ducts of sample D were created by drilling 20 holes in the yoke to produce 4 groups of axial ducts in the yoke of an Al die-cast rotor, as shown in Fig. 7(a). A fabricated Cu bar rotor with $N_d = 4$ shown in Fig. 7(b) was designed and built from the laser cut laminations of Fig. 7(c) to fit the stator of sample D, as it is representative of HV motors.

The stators of samples D, E, and F1 have 36 stator slots with 7/9 fractional pitch. To observe how the space harmonic content of the stator winding influences the increase in $f_{brb,h}$, one of the 380-V 5.5-kW stators identical to samples D, E, and F1 was rewound with a full pitch winding (sample F2) with the same number of turns. The stator structure and pitch factor for the

TABLE III
STATOR WINDING STRUCTURE AND PITCH FACTOR FOR FUNDAMENTAL, FIFTH, AND SEVENTH SPACE HARMONICS FOR SAMPLES D, E, AND F

| Sample | N_s | N_r | Coil pitch | $ k_{p,1} $ | $ k_{p,5} $ | $ k_{p,7} $ |
|----------|-------|-------|----------------------------|-------------|-------------|-------------|
| D, E, F1 | 36 | 44 | 140°, 7/9 fractional pitch | 0.940 | 0.174 | 0.776 |
| F2 | 36 | 44 | 180°, full pitch | 1 | 1 | 1 |

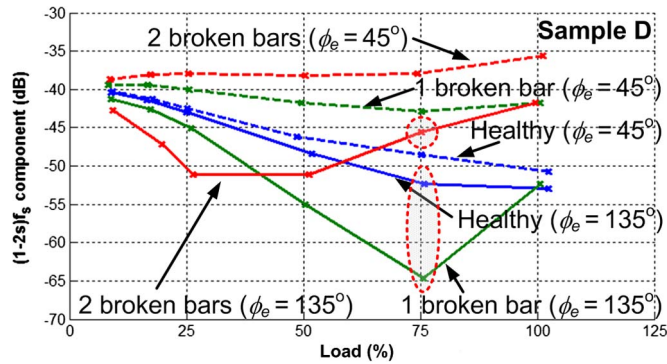


Fig. 8. MCSA measurements of $(1 - 2s)f_s$ components as a function of % rated slip (load) with zero to two broken bars (sample D) located at $\phi_e = 45^\circ$ (dotted line) and $\phi_e = 135^\circ$ (real line).

fundamental, fifth, and seventh space harmonics for samples D, E, and F are summarized in Table III.

For samples D, E, and F, up to 3 of 44 contiguous *Al* or *Cu* bars were cut at the bar and end ring joint to simulate broken bars. To test under the condition where the $i_{m,brb,1}$ and $i_{r,brb,1}$ components are in phase (add), bars at the $\phi_e = 45^\circ$ location shown in Fig. 4(b) were cut. The case where the $i_{m,brb,1}$ and $i_{r,brb,1}$ components are out of phase (cancel, $\phi_e = 135^\circ$) was also tested by rotating the same rotor used for the $\phi_e = 45^\circ$ case in the opposite direction. This is equivalent to the broken bar being located at $\phi_e = 135^\circ$. The test results for the healthy rotor are different in Figs. 8, 10, 11, and 13 for the cases of $\phi_e = 45^\circ$ and $\phi_e = 135^\circ$ for this reason. It was not possible to damage the rotor bars of samples B or C since they are HV motors operating in the field. The information regarding the rotors and test results for motor samples A–F is summarized in Table I. The load of the motor was controlled by adjusting the field voltage of a 22.5-kW dc generator coupled to the motor. Commercial current sensors and a data acquisition board were used to measure the current at 6 kHz sampling for 60 s under steady-state conditions with MCSA.

B. Experimental Results

MCSA testing was performed with the motor operating under 10%–100% rated load with zero to two broken bars located at $\phi_e = 45^\circ$ and 135° for samples D and E (healthy rotor refers to the rotor with zero broken bars). The interaction between the broken bar and axial duct influence can be seen in the measurements of the $(1 - 2s)f_s$ components of sample D in Fig. 8. It can be observed that $I_{s,brb,1}$ increases if the bar is broken at the $\phi_e = 45^\circ$ location [Fig. 3(a)] because the $i_{m,brb,1}$ and $i_{r,brb,1}$ components are in phase (add). $I_{s,1-2s}$ decreases (and then increases) if $\phi_e = 135^\circ$ because $i_{m,brb,1}$

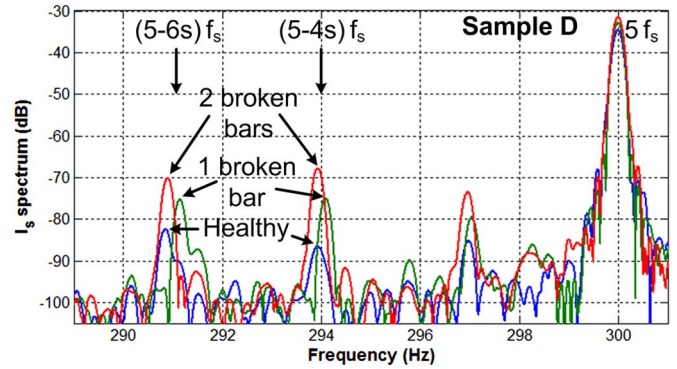


Fig. 9. I_s spectrum showing $(5 - 4s)f_s$ and $(5 - 6s)f_s$ components with zero to two broken bars (sample D) located at $\phi_e = 135^\circ$ at 75% rated load.

and $i_{r,brb,1}$ are out of phase (cancel). The pattern of $I_{s,brb,1}$ in Fig. 8 is consistent with the simulated results shown in Fig. 4 and shows that $I_{s,brb,1}$ is not a reliable indicator since it can change depending on the fault location, load, and amplitude of individual $I_{m,brb,1}$ and $I_{r,brb,1}$ components.

The $(5 - 4s)f_s$ and $(5 - 6s)f_s$ components in the I_s spectrum are shown in Fig. 9 for sample D for the case where zero, one, and two bars are broken at $\phi_e = 135^\circ$ under 75% rated load. This corresponds to the 75% rated load condition with zero to two broken bars highlighted in Fig. 8, where MCSA based on $I_{s,brb,1}$ fails. Under this condition, the rotor is likely to be misdiagnosed as “faulty” (−52.3 dB) when the rotor is healthy and as “healthy” (−64.6 dB) when the rotor has one broken bar. It can be seen in Fig. 9 that the $(5 - 4s)f_s$ and $(5 - 6s)f_s$ components increase with the number of broken bars unlike the $(1 - 2s)f_s$ component.

The $f_{brb,h}$ components induced by the fifth and seventh space harmonics $(5 - 4s)f_s$, $(7 - 6s)f_s$, $(5 - 6s)f_s$, and $(7 - 8s)f_s$ were observed under different load and fault conditions, and all of the components showed a similar trend in that they increase with fault severity. It was concluded after careful observation that the $(5 - 4s)f_s$ component provides the most consistent and reliable indication of rotor faults. The average of the $(5 - 4s)f_s$ components obtained three times under 25%–100% rated load with zero to two broken bars located at $\phi_e = 45^\circ$ and 135° for sample D is shown in Fig. 10. It can be clearly seen that the fault indicator $(5 - 4s)f_s$ increases with the number of broken bars independent of fault location and load. This shows that the proposed method provides reliable detection of rotor faults and is immune to the axial duct influence.

The results shown in Figs. 8–10 for sample D are repeated for sample E in Figs. 11–13. The trend in how the $N_d = N_p$ axial ducts influence $I_{s,brb,1}$ and how the $f_{brb,h}$ components change with fault severity is similar to that of sample D. It can be observed in Fig. 11 that the influence of axial ducts is smaller for the case of sample E (smaller $I_{m,brb,1}$). This is due to the narrower flux path behind the axial duct, which shows that the degree of the axial duct interference depends on the rotor axial duct design. For the case where the motor is operating at 25% rated load with the rotor fault located at $\phi_e = 135^\circ$ (highlighted in Fig. 11), the $(1 - 2s)f_s$ component

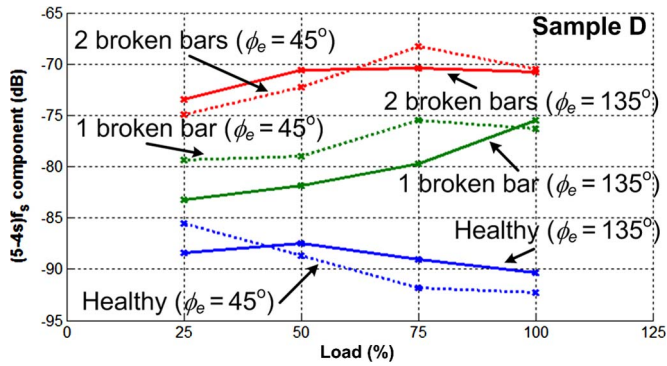


Fig. 10. MCSA measurements of $(5 - 4s)f_s$ components as a function of % rated slip (load) with zero to two broken bars (sample D) located at $\phi_e = 45^\circ$ (dotted line) and $\phi_e = 135^\circ$ (real line).

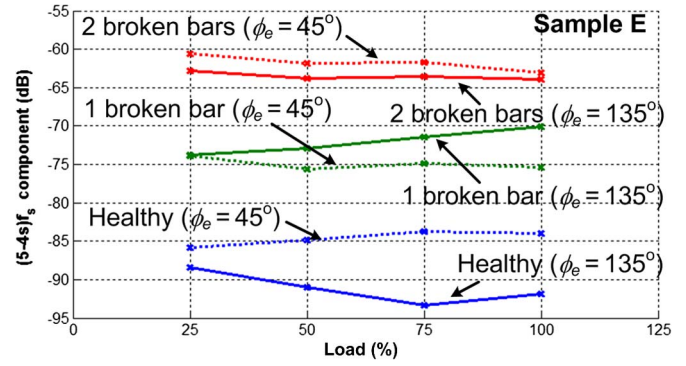


Fig. 13. MCSA measurements of $(5 - 4s)f_s$ components as a function of % rated slip (load) with zero to two broken bars (sample E) located at $\phi_e = 45^\circ$ (dotted line) and $\phi_e = 135^\circ$ (real line).

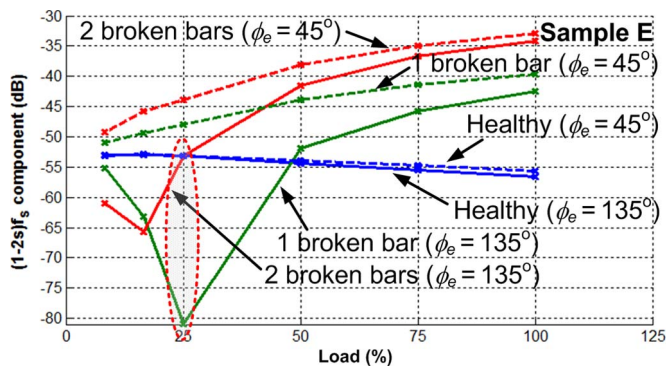


Fig. 11. MCSA measurements of $(1 - 2s)f_s$ components as a function of % rated slip (load) with zero to two broken bars (sample E) located at $\phi_e = 45^\circ$ (dotted line) and $\phi_e = 135^\circ$ (real line).

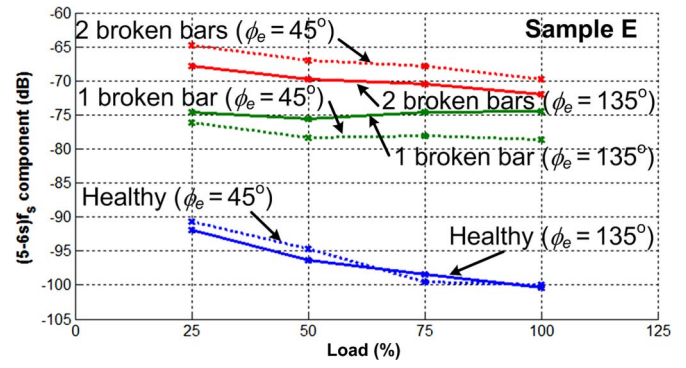


Fig. 14. MCSA measurements of $(5 - 6s)f_s$ components as a function of % rated slip (load) with zero to two broken bars (sample E) located at $\phi_e = 45^\circ$ (dotted line) and $\phi_e = 135^\circ$ (real line).

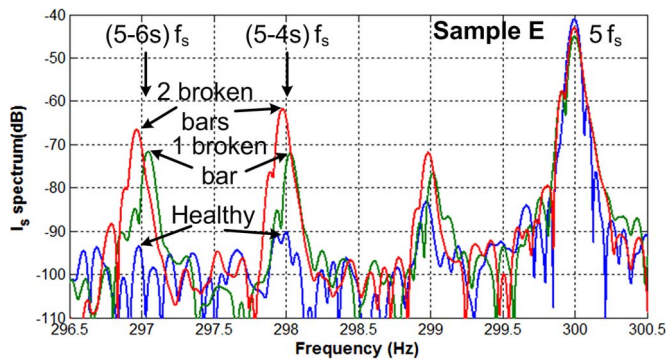


Fig. 12. I_s spectrum showing $(5 - 4s)f_s$ and $(5 - 6s)f_s$ components with zero to two broken bars (sample E) located at $\phi_e = 135^\circ$ at 25% rated load.

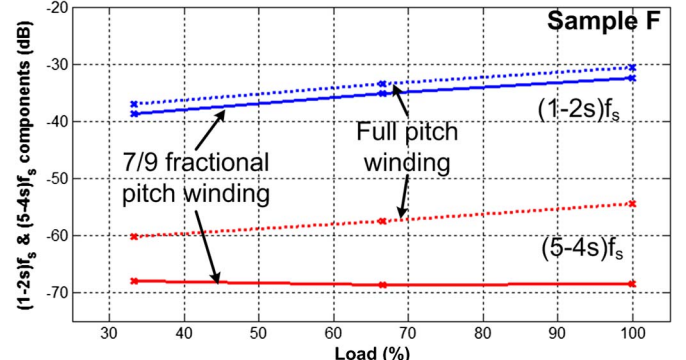


Fig. 15. MCSA measurements of $(1 - 2s)f_s$ and $(5 - 4s)f_s$ components for fractional pitch (sample F1) and full pitch (sample F2) winding with three broken rotor bars.

is relatively high at -53.1 dB for a healthy rotor and low at -81.0 dB for a rotor with one broken bar. It is shown in Fig. 12 that the $(5 - 4s)f_s$ and $(5 - 6s)f_s$ components increase with fault severity, providing reliable detection of rotor faults where MCSA based on $(1 - 2s)f_s$ produces false indications. The $(5 - 4s)f_s$ and $(5 - 6s)f_s$ components under 25%–100% rated load with zero to two broken bars located at $\phi_e = 45^\circ$ and 135° are shown in Figs. 13 and 14, respectively, for sample E. The $(5 - 4s)f_s$ and $(5 - 6s)f_s$ components show a clear increase with fault severity independent of fault location and load level, as in the case of sample D.

The $(1 - 2s)f_s$ and $(5 - 4s)f_s$ components measured from samples F1 and F2 with 7/9 fractional pitch and full pitch stator winding with three broken rotor bars are shown in Fig. 15 to demonstrate one of the limitations of the proposed method. The rotor of sample F is the same as the Al die cast rotor of sample D but without any axial ducts. It can be observed that the increase in the $(1 - 2s)f_s$ and $(5 - 4s)f_s$ components is larger for the full pitch winding since the fundamental and fifth space harmonic components are relatively larger, as can be seen in Table III. The $(1 - 2s)f_s$ and $(5 - 4s)f_s$ components are typically below -60 and -80 dB, respectively,

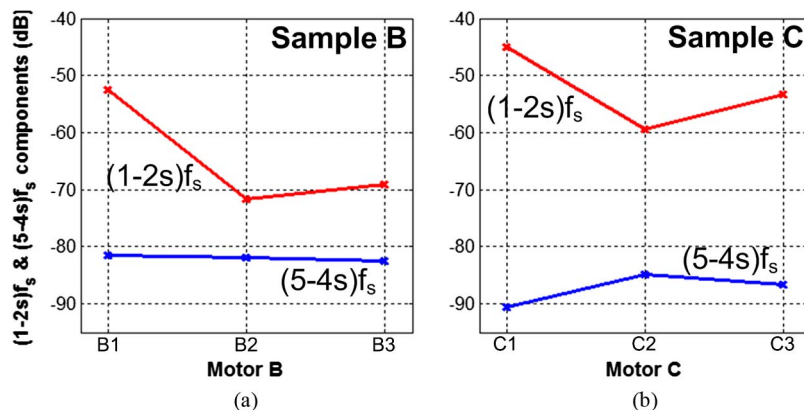


Fig. 16. MCSA measurements of $(1 - 2s)f_s$ and $(5 - 4s)f_s$ components for motors with false rotor fault alarms. (a) Motor samples B1, B2, and B3. (b) Motor samples C1, C2, and C3.

when measured for healthy motors, as can be seen in Figs. 10 and 13. The difference in the increase is substantial for the $(5 - 4s)f_s$ component, where the pitch factor is higher for the full pitch winding by 10–15 dB. The results of Fig. 15 show that the increase in the fault indicator depends on the stator winding structure, and this is one of the potential limitations of determining fault severity based on the $f_{brb,h}$ components. The results shown in Figs. 10, 13, and 15 also show that the amplitude of the $f_{brb,h}$ components are insensitive to load compared to the $f_{brb,1}$ components, which is an advantage.

The $(5 - 4s)f_s$ and $(1 - 2s)f_s$ components of the 6.6-kV 350-kW and 280-kW motor samples B and C of Fig. 2 with false rotor fault alarms are shown in Fig. 16. The $(5 - 4s)f_s$ components for identical motors B1, B2, and B3 were measured at -81.5 , -81.8 , and -82.6 dB, respectively. This is very consistent compared to the $(1 - 2s)f_s$ components that have a variation of 20 dB, as shown in Figs. 3(b) and 16(a). A similar trend can be observed for motors C1, C2, and C3, where the $(5 - 4s)f_s$ components are very low and consistent at -90.5 , -84.8 , -86.6 dB compared to the $(1 - 2s)f_s$ components that have a variation of 15 dB. In fact, the $(5 - 4s)f_s$ component of motor C1 with the highest $(1 - 2s)f_s$ component is the lowest, as can be seen in Figs. 3(c) and 16(b). The results of Fig. 16 show that inspection of the rotor due to the false indications produced by the $(1 - 2s)f_s$ component could have been avoided if the $(5 - 4s)f_s$ component had been monitored. If the proposed method had been applied for screening out the false alarm, the plant that disassembled sample C could have saved 20 000 USD on motor inspection. The test results on the 6.6-kV motor (samples B and C) and the laboratory samples (samples D, E, and F) clearly show that false rotor fault alarms can be avoided by analyzing the $f_{brb,h}$ component with MCSA.

V. CONCLUSION

Online monitoring of space-harmonic-induced rotor fault components $f_{brb,h}$ with MCSA has been proposed as a reliable means of detecting rotor faults independent of axial ducts. Motor outage and inspection due to false indications produced by axial ducts is currently a common problem in the field with no solution other than offline or startup testing. An analysis shows that space harmonic flux cannot penetrate into the rotor to produce false alarms due to the high slip between the rotor and

space harmonic wave, making the $f_{brb,h}$ components a reliable fault indicator. The effectiveness of the proposed method was verified on custom-built rotors and also on 6.6-kV motors in the field that were misdiagnosed with rotor faults. The experimental results clearly show that the proposed fault indicator is immune to the axial duct influence and can be used in detecting the fault and screening out false alarms. The trend of the 1) increase in the $f_{brb,h}$ components with time and 2) comparison of the $f_{brb,h}$ components measured on motors of identical design can be used as an effective measure of false alarms.

The space harmonics ($f_{brb,h}$) based MCSA method, which has been applied to this problem for the first time in this work, is expected to help prevent unnecessary inspection and/or loss of production due to false broken bar indications that frequently occur in the field. It also provides reliable diagnosis of motors with axial-duct-induced magnetic asymmetry, which was only possible with offline or startup test methods. The proposed algorithm is currently being successfully applied in the field for screening out false-positive indications when the $(1 - 2s)f_s$ broken bar frequency component of online MCSA exceeds the alarm level.

REFERENCES

- [1] C. Concari, G. Franceschini, C. Tassoni, and A. Toscani, "Validation of a faulted rotor induction machine model with an insightful geometrical interpretation of physical quantities," *IEEE Trans. Ind. Electron.*, vol. 60, no. 9, pp. 4074–4083, Sep. 2013.
- [2] Y. Kim, Y. Youn, D. Hwang, J. Sun, and D. Kang, "High-resolution parameter estimation method to identify broken rotor bar faults in induction motors," *IEEE Trans. Ind. Electron.*, vol. 60, no. 9, pp. 4103–4117, Sep. 2013.
- [3] A. Soualhi, G. Clerc, and H. Razik, "Detection and diagnosis of faults in induction motor using an improved artificial ant clustering technique," *IEEE Trans. Ind. Electron.*, vol. 60, no. 9, pp. 4053–4062, Sep. 2013.
- [4] G. B. Kliman, R. A. Koegl, J. Stein, R. D. Endicott, and M. W. Madden, "Noninvasive detection of broken rotor bars in operating induction motors," *IEEE Trans. Energy Convers.*, vol. 3, no. 4, pp. 873–879, Dec. 1988.
- [5] W. Thomson, "Recent (2005–2006) case histories on the application of motor current signature analysis to detect broken rotor bars," in *Proc. IRMC*, Toronto, ON, Canada, 2006.
- [6] I. M. Culbert and W. Rhodes, "Using current signature analysis technology to reliably detect cage winding defects in squirrel-cage induction motors," *IEEE Trans. Ind. Appl.*, vol. 43, no. 2, pp. 422–428, Mar./Apr. 2007.
- [7] W. T. Thomson, "On-line current monitoring—The influence of mechanical loads or a unique rotor design on the diagnosis of broken rotor bars in induction motors," in *Proc. ICEM*, 1992, pp. 1236–1240.

- [8] A. Bellini *et al.*, "On-field experience with on-line diagnosis of large induction motors cage failures using MCSA," *IEEE Trans. Ind. Appl.*, vol. 38, no. 4, pp. 1045–1053, Jul./Aug. 2002.
- [9] S. Lee *et al.*, "Evaluation of the influence of rotor axial air duct design on condition monitoring of induction motors," *IEEE Trans. Ind. Appl.*, vol. 49, no. 5, pp. 2024–2033, Oct. 2013.
- [10] C. Yang *et al.*, "Reliable detection of induction motor rotor faults under the rotor axial air duct influence," in *Proc. IEEE ECCE*, Raleigh, NC, USA, Sep. 2013, pp. 2508–2515.
- [11] B. D. Evans, "Induction motor case histories: A focus on electrically related phenomena," in *Proc. Vib. Inst. Annu. Meet.*, Harrisburg, PA, USA, 2009.
- [12] *Testing of Squirrel Cage Rotors*, EASA AR100-2010, Oct. 2010.
- [13] T. A. Lipo, *Introduction to AC Machine Design*. Madison, WI, USA: Wisconsin Power Electron. Res. Center, Univ. Wisconsin, 2004.
- [14] T. J. Sobczyk and W. Maciolek, "Diagnostics of rotor-cage faults supported by effects due to higher MMF harmonics," in *Proc. IEEE Power Tech Conf.*, Jun. 2003, vol. 2, pp. 1–5.
- [15] M. Riera-Guasp, J. Pons-Llinares, F. Vedreno-Santos, J. A. Antonino-Daviu, and M. Fernandez Cabanas, "Evaluation of the amplitudes of high-order fault related components in double bar faults," in *Proc. IEEE Int. Symp. Diagnost. Elect. Mach., Power. Electron. Drives*, Sep. 2011, pp. 307–315.
- [16] H. Henao, H. Razik, and G. A. Capolino, "Analytical approach of the stator current frequency harmonics computation for detection of induction machine rotor faults," *IEEE Trans. Ind. Appl.*, vol. 41, no. 3, pp. 801–807, May/Jun. 2005.
- [17] B. Akin, U. Orguner, H. A. Toliyat, and M. Rayner, "Low order PWM inverter harmonics contributions to the inverter-fed induction machine fault diagnosis," *IEEE Trans. Ind. Electron.*, vol. 55, no. 2, pp. 610–619, Feb. 2008.
- [18] C. H. De Angelo, G. R. Bossio, J. M. Bossio, and G. O. Garcia, "Broken bar detection in single-phase reciprocating compressors," in *Proc. IEEE Ind. Electron. Conf.*, Nov. 2008, pp. 1125–1130.
- [19] C. Bruzzese, "Analysis and application of particular current signatures (symptoms) for cage monitoring in nonsinusoidally fed motors with high rejection to drive load, inertia, frequency variations," *IEEE Trans. Ind. Electron.*, vol. 55, no. 12, pp. 4137–4155, Dec. 2008.
- [20] G. M. Joksimovic, J. Riger, T. M. Wolbank, N. Peric, and M. Vasak, "Stator-current spectrum signature of healthy cage rotor induction machines," *IEEE Trans. Ind. Electron.*, vol. 60, no. 9, pp. 4025–4033, Sep. 2013.
- [21] S. H. Kia, H. Henao, and G.-A. Capolino, "Some digital signal processing techniques for induction machines diagnosis," in *Proc. IEEE SDEMPED*, Sep. 2011, pp. 322–329.
- [22] M. Y. Kaikaa and M. Hadjami, "Effects of the simultaneous presence of static eccentricity and broken rotor bars on the stator current of induction machine," *IEEE Trans. Ind. Electron.*, vol. 61, no. 5, pp. 2452–2463, May 2014.



Chanseung Yang (S'12) received the B.S. degree in electrical engineering from Korea University, Seoul, Korea, in 2012, where he is currently working toward the Ph.D. degree.

In 2012, he was an Intern with the Universitat Politècnica de València (UPV), Valencia, Spain. In 2014, he was an Intern with the University of Bologna, Bologna, Italy. His research interests are condition monitoring and analysis of electric machinery.



Tae-June Kang (S'11) received the B.S. degree in electrical engineering from Korea University, Seoul, Korea, in 2011, where he is currently working toward the Ph.D. degree in electrical engineering.

He was an Intern with the Universitat Politècnica de València (UPV), Valencia, Spain, in 2012, and an Intern with the Universitat di Bologna, Bologna, Italy, in 2014. His research interests are stator winding insulation testing and condition monitoring and diagnostics of

electric machinery.



Sang Bin Lee (S'95–M'01–SM'07) received the B.S. and M.S. degrees in electrical engineering from Korea University, Seoul, Korea, in 1995 and 1997, respectively, and the Ph.D. degree in electrical engineering from Georgia Institute of Technology, Atlanta, GA, USA, in 2001.

From 2001 to 2004, he was with the General Electric Global Research Center, Schenectady, NY, USA, where he developed an interlaminar core fault detector for generator stator cores and worked on insulation quality assessment for electric machines. From 2010 to 2011, he was a Research Scientist with the Austrian Institute of Technology, Vienna, Austria, where he worked on condition monitoring of PM synchronous machines. Since 2004, he has been a Professor of electrical engineering with Korea University. His current research interests are protection, monitoring and diagnostics, and analysis of electric machines and drives.

Dr. Lee was the recipient of nine prize paper awards from the IEEE Power Engineering Society, the Electric Machines Committee of the IEEE Industry Applications Society (IAS), and the Technical Committee on Diagnostics of the IEEE Power Electronics Society. He serves as a Distinguished Lecturer (2014–2015) for IEEE IAS and as an Associate Editor of the IEEE TRANSACTIONS ON INDUSTRY APPLICATIONS for the IEEE IAS Electric Machines Committee.



Ji-Yoon Yoo received the B.S. and M.S. degrees in electrical engineering from Korea University, Seoul, Korea, in 1977 and 1983, respectively, and the Ph.D. degree in electrical engineering from Waseda University, Tokyo, Japan, in 1987.

From 1987 to 1991, he was an Assistant Professor with the Department of Electrical Engineering, Changwon National University, Changwon, Korea. Since 1991, he has been with the Department of Electrical Engineering,

Korea University, where he is currently involved in research on control of electric machines and drives, and power electronics converters. His research interests include modeling, analysis, and control of hybrid electric vehicle systems and flexible ac transmission systems.



Alberto Bellini (S'96–M'99) was born in Italy in 1969. He received the Laurea (M.S.) degree in electronic engineering and the Ph.D. degree in computer science and electronics engineering from the University of Bologna, Bologna, Italy, in 1994 and 1998, respectively.

From 1999 to 2004, he was with the University of Parma, Parma, Italy. He was an Honorary Scholar with the University of Wisconsin–Madison, Madison, WI, USA, in 2000. From 2004 to 2013, he was with the University of

Modena and Reggio Emilia, Reggio Emilia, Italy. Since 2013, he has been a Professor of electric machines and drives with the Department of Electrical Engineering, University of Bologna. He is the author or coauthor of more than 80 papers and one textbook and is the holder of three industrial patents. His research interests include electric drive design and diagnosis, power electronics, and signal processing for industrial applications and audio.

Dr. Bellini serves as an Associate Editor of the IEEE TRANSACTIONS ON INDUSTRIAL ELECTRONICS. He was the recipient of the First Prize Paper Award from the Electric Machines Committee of the IEEE Industry Applications Society in 2001.



Luca Zarri (M'05–SM'12) was born in Bologna, Italy, in 1972. He received the M.Sc. degree in electrical engineering (with honors) and the Ph.D. degree from the University of Bologna, Bologna, in 1998 and 2007, respectively.

He was a freelance software programmer from 1989 to 1992 and a plant designer with an engineering company from 1998 to 2002. In 2003, he became a Laboratory Engineer with the Department of Electrical Engineering, University of Bologna, where he has been an

Assistant Professor since 2005. He is the author or coauthor of more than 100 scientific papers. His research activity concerns the control of power converters and electric drives.

Dr. Zarri is a member of the IEEE Industry Applications, IEEE Power Electronics, and IEEE Industrial Electronics Societies. He serves as an Associate Editor for the IEEE TRANSACTIONS ON INDUSTRY APPLICATIONS for the IEEE IAS Electric Machines Committee and has served as a Guest Associate Editor for some special issues of the IEEE TRANSACTIONS ON INDUSTRY APPLICATIONS and IEEE JOURNAL OF EMERGING AND SELECTED TOPICS IN POWER ELECTRONICS.



Fiorenzo Filippetti (M'00) received the M.S. degree in electrical engineering from the University of Bologna, Bologna, Italy, in 1970.

In 1976, he became an Assistant Professor with the Department of Electrical, Electronics and Information Engineering “G. Marconi (DEI),” University of Bologna, where he is currently a Full Professor of electrical machines. He was a Visiting Professor with the University Claude Bernard, Centre de Génie Electrique de Lyon (CEGELY), University Claude Bernard, Lyon,

France, and the University of Picardie Jules Verne, Amiens, France. His main research interests include simulation and modeling of electric circuits and systems, and the study and application of condition-monitoring and fault-detection techniques for ac electrical machines.

Prof. Filippetti was the recipient of the IEEE PELS Diagnostic Achievement Award in 2013 and three Prize Paper Awards at IEEE IAS and SDEMPED conferences.